Pickering emulsion of ginger essential oil stabilized by zein-tannic acid-gum Arabic ternary nanoparticles: Application in the development of active films based on xylan/sodium alginate/ polyvinyl alcohol

Junhan Liu, Marie-Laure Fauconnier, Aurore Richel, Wenqing Zhu, Wenjing Yang, Yanna Hu, Yuhong Jin

PII: S0308-8146(26)00448-6

DOI: https://doi.org/10.1016/j.foodchem.2026.148290

Reference: FOCH 148290

To appear in: *Food Chemistry*

Received date: 30 June 2025

Revised date: 5 January 2026

Accepted date: 2 February 2026

Please cite this article as: J. Liu, M.-L. Fauconnier, A. Richel, et al., Pickering emulsion of ginger essential oil stabilized by zein-tannic acid-gum Arabic ternary nanoparticles: Application in the development of active films based on xylan/sodium alginate/ polyvinyl alcohol, *Food Chemistry* (2024), https://doi.org/10.1016/j.foodchem.2026.148290

Pickering emulsion of ginger essential oil stabilized by zein-tannic acid-gum Arabic ternary nanoparticles: Application in the development of active films based on xylan/sodium alginate/ polyvinyl alcohol

Junhan Liu [a, b, c], Marie-Laure Fauconnier [b], Aurore Richel [c], Wenqing Zhu [a, b, c], Wenjing Yang [a], Yanna Hu [a], Yuhong Jin [a, *]

[a] Key Laboratory of Food Processing Technology and Quality Control in Shandong Province, College of Food Science and Engineering, Shandong Agricultural University, Tai'an 271018, China.

[b] Laboratory of Chemistry of Natural Molecules, Gembloux Agro-Bio Tech, University of Liège, Passage des déportés 2, B-5030, Gembloux, Belgium.

[c] Laboratory of Biomass and Green Technologies, Gembloux Agro-Bio Tech, University of Liège, Passage des déportés 2, B-5030, Gembloux, Belgium.

*Corresponding author: yuhongjin79@sdau.edu.cn

Abstract

In this study, ternary biopolymer nanoparticles comprising zein, tannic acid, and gum Arabic (ZTGs) were synthesized to stabilize ginger essential oil Pickering emulsion (GOPE). The stabilized GOPE was blended with a xylan/sodium alginate/polyvinyl alcohol matrix to prepare active films. GOPE stabilized by ZTGs with near-medium wettability ($\theta_{o/w}$ = 94.15 ± 0.35°) exhibited outstanding stability, particularly at an oil volume fraction (φ) of 0.5, where emulsion gel formation was observed. Furthermore, GOPE demonstrated excellent compatibility with the film-forming matrix. Incorporating GOPE markedly enhanced the thermal stability, UV-shielding, and water resistance of the films, and enabled the controlled release of ginger essential oil from the matrix. Moreover, films containing GOPE exhibited remarkable antioxidant activity and demonstrated antibacterial effects against foodborne pathogens (*Escherichia coli* and *Staphylococcus aureus*) as well as spoilage bacteria (*Pseudomonas aeruginosa* and *Bacillus subtilis*). These functional properties contributed to delaying strawberry decay and maintaining fruit quality.

Keywords

Ternary nanoparticles, Pickering emulsions, Active films, Fruit preservation

1. Introduction

Currently, biobased active films incorporated with functional bioactive compounds have attracted increasing attention as promising candidates for next-generation food packaging materials. Among these bioactive agents, essential oils (EOs) extracted from plants are widely applied in biobased active films owing to their outstanding antioxidant and antimicrobial activities (Wang et al., 2024b). However, the high volatility and strong hydrophobicity of EOs result in poor dispersion within hydrophilic film matrices. Although surfactants such as Tween and Span have been extensively used to improve EO dispersion (Acharya et al., 2024; Mutlu, 2023; Pérez-Córdoba et al., 2018; Zhang et al., 2021), their limited loading capacity, inability to effectively suppress EO volatilization, and potential cytotoxicity restrict their suitability for food packaging applications (Liu et al., 2019a; Kaur & Mehta, 2017).

In recent years, solid particle–stabilized Pickering emulsions have emerged as a highly promising strategy for fabricating EO-loaded active films (Zhao et al., 2024). Among various solid particles used as Pickering stabilizers, zein has been extensively employed due to its high content of nonpolar amino acids and its ability to form nanoparticles via antisolvent precipitation (Liang et al., 2021). However, zein nanoparticles alone exhibit insufficient interfacial adsorption at the oil–water interface, leading to inadequate emulsion stability (de Folter et al., 2012), which limits their direct application in active films. To overcome this limitation, hydrophilic polysaccharides such as pectin (Jiang et al., 2020; Wang et al., 2023a), gum Arabic (GA) (Gali et al., 2022; Li et al., 2018b), hyaluronic acid (Zhang et al., 2024b), and karaya gum (Wu et al., 2022) have been commonly employed to coat zein nanoparticles, thereby improving their wettability and enhancing Pickering emulsion stability. Among these polysaccharides, GA has received considerable attention as a low-cost natural anionic polysaccharide. Multiple studies have demonstrated that Pickering emulsions stabilized by zein–GA nanoparticles can serve as stable carriers when incorporated into polymer matrices, enabling effective regulation of the spatial distribution and release behavior of active

compounds and thereby significantly improving the functional performance of active films (Pu et al., 2024; Cao et al., 2024). Nevertheless, zein–GA nanoparticles are highly sensitive to ionic microenvironments, particularly in the presence of salts, which may induce desorption of GA from the zein particle surface and ultimately result in Pickering emulsion destabilization (Chen et al., 2019). Tannic acid (TA), a polyphenolic compound rich in hydroxyl groups, can interact noncovalently with zein through hydrogen bonding and hydrophobic interactions, thereby improving the interfacial properties of colloidal particles (Li et al., 2023b; Liang et al., 2021). Moreover, TA is expected to promote the formation of more stable core–shell structures in combination with zein and GA (Zhang et al., 2022). In recent studies, ternary complexes composed of zein, polyphenols, and polysaccharides have been demonstrated to produce highly stable Pickering emulsions (Najari et al., 2024). Pickering emulsions stabilized by such ternary nanoparticles exhibit superior interfacial stability, higher bioactive compound loading capacity, and enhanced resistance to coalescence, Ostwald ripening, and volatilization, showing strong potential in 3D printing and delivery systems (Liu et al., 2023; Zhou et al., 2024; Li et al., 2023a). These enhanced properties are also highly desirable for improving the applicability and performance reliability of active films. To the best of our knowledge, however, the application of Pickering emulsions stabilized by ternary nanoparticles composed of zein, polyphenols, and polysaccharides in active films has rarely been reported.

Based on the aforementioned considerations, ternary nanoparticles composed of zein, tannic acid, and gum Arabic (ZTGs) were prepared and characterized in this study. These ZTGs were employed to stabilize ginger essential oil Pickering emulsions (GOPE), which were subsequently incorporated at different concentrations into a film-forming matrix composed of xylan, sodium alginate, and PVA. The effects of GOPE incorporation on the mechanical properties, barrier performance, thermostability, antioxidant activity, and antimicrobial activity of the active films were systematically evaluated. Additionally, the potential application of the developed active films in preserving fruit freshness was investigated. This work establishes an effective strategy

for active packaging by constructing highly stable Pickering emulsions via ternary nanoparticles.

2. Materials and methods

2.1. Materials and chemicals

Corn cob-derived xylan (CAS 9014-63-5, purity 95%), sodium alginate (CAS 9005-38-3, M/G ratio = 1:1, purity 90%), zein (CAS 9010-66-6), and tannic acid (CAS 1401-55-4, purity 98%) were provided by Macklin Biochemical Co., Ltd. (Shanghai, China). Polyvinyl alcohol (CAS 9002-89-5, PVA 1799, alcoholysis degree $\geqslant$97%) was ordered from Sinopharm Chemical Reagent Co., Ltd. (Shanghai, China). Ginger essential oil (GEO) was purchased from Huashuo Spice Oil Co., Ltd. (Jiangxi, China). Gum Arabic (CAS 9000-01-5, AR analytical grade) was sourced from Shanghai Yuanye Biotechnology Co., Ltd. (Shanghai, China). The bacterial strains *Staphylococcus aureus* ATCC12598, *Pseudomonas aeruginosa* ATCC27853, *Escherichia coli* ATCC25922, and *Bacillus subtilis* ATCC6051 were purchased from Shanghai Luwei Technology Co., Ltd. (Shanghai, China). Strawberries were bought from a local market (Tai'an, Shandong, China) without any preservation treatment.

2.2. Preparation of Zein-TA-GA ternary nanoparticles (ZTGs)

ZTGs were prepared according to the methods described by Li et al. (2023b) and Dai et al. (2018), with the introduction of an additional ultrasonication step to promote nanoparticle formation. Briefly, 1 g of zein powder was solubilized in 40 mL of 85% ethanol and stirred at room temperature for 3 h. Then, 0.2 g of tannic acid (TA) powder was added to the zein solution, and the mixture was stirred for an additional hour under light-protected conditions. The resulting solution was rapidly dripped into 120 mL of deionized water (pH 5.0), followed by 10-min ultrasonication at 600 W. To concentrate the particles, a rotary evaporator (N-1300, EYELA, Japan) was used to evaporate all ethanol and part of water until the concentration of particle was 2% (w/v), forming the ZTs. The ZTs were then combined with gum Arabic (GA) solution (2% w/v, pH 5.0) at

a 1:1 volume ratio under stirring to produce the ZTGs dispersion. Detailed characterization methods for ZTGs can be found in Section 1 of the Supplementary Materials.

2.3. Preparation of ZTGs stabilized GOPE

Pickering emulsions were formulated by mixing ZTGs dispersions with oils at varying oil volume fractions (φ = 0.3, 0.4, 0.5, 0.6, and 0.75) while maintaining a constant total emulsion volume of 30 mL. The ZTGs dispersion was thoroughly mixed with GEO and emulsified with a high-shear disperser (ULTRA TURRAX® T18, IKA, Germany), which was operated at 15,000 rpm for 5 min to produce GOPE. The characterization of GOPE included droplet size analysis, morphological observations, and rheological property measurements, as described in Section 2 of the Supplementary Materials.

2.4. Preparation of composite films

The procedure was referred to the report of Liu et al. (2024), with modifications. Briefly, PVA particles (1.0 g) was added to deionized water (100 mL) and heated to 95 °C on a magnetic stirring bar, stirring continuously until a homogeneous PVA solution was generated. The solution was then cooled to 60 °C, and 0.5 g of xylan followed by 0.5 g of sodium alginate were added. To ensure complete dissolution, the mixture was stirred for 90 min. Afterward, the solution was further cooled to 40 °C, and glycerol (20% of the combined weight of xylan, sodium alginate, and PVA) was added as a plasticizer. The mixture was stirred for an additional 60 min to prepare the film-forming solution. GOPE (φ = 0.5) was incorporated into the film-forming solution at different concentrations: 0.0%, 0.5%, 1.0%, 1.5%, and 2.0% (w/w). The mixtures were homogenized at 12,000 rpm for 2 min to produce the active film-forming solutions. After vacuum degassing for 1 h, 30 g of each solution was cast onto a polystyrene mold (10 cm × 10 cm) and dried for 14 h at 35 °C. The composite films were carefully peeled off the molds and labeled as XL/SA/PVA, XL/SA/PVA-0.5%GOPE, XL/SA/PVA-

1.0%GOPE, XL/SA/PVA-1.5%GOPE, and XL/SA/PVA-2.0%GOPE. Before analysis, all films were conditioned at 25 ± 1 °C and 50 ± 2% relative humidity (RH) for 2 d.

2.5. Structural characterization of film

A field-emission scanning electron microscope (JSM-7800F, JEOL, Japan) was used to analyze the cross-sectional and surface morphologies of the films. The samples were frozen in liquid nitrogen and then fractured to expose their internal structure. Surface roughness was measured using a 3D optical profiler (UP-24, Rtec Instruments, USA). Fourier-transform infrared (FTIR) spectra were recorded using a Nicolet iS10 spectrometer (Thermo Fisher Scientific, USA) over the range of 4000–400 cm^{-1}, with 64 scans performed at a resolution of 4 cm^{-1}. X-ray diffraction (XRD) analysis was performed on a D8 ADVANCE diffractometer (Bruker, Germany) at a scanning rate of 5°/min across a 2θ range of 5°–50° to evaluate the crystallinity. Molecular interactions within the film matrix were investigated using AutoDock Vina. The 3D structures of xylan, sodium alginate, and PVA (PubChem CIDs: 129539666, 133126842, and 11199, respectively) were obtained from PubChem, and PyMol 2.5.4 was used to visualize the docking results.

2.6. Performance of composite films

2.6.1. Optical characteristics

The color index of the films was measured using a colorimeter (CR-400, Konica Minolta Co., Ltd., Japan), with a white standard plate (L* = 92.89, a* = 0.72, b* = 0.35) used as the background reference. Light transmittance (200-800 nm) was recorded using a UV-Vis spectrophotometer (UV-2600i, Shimadzu, Japan), following the procedure outlined by Li et al. (2024b).

2.6.2. Mechanical performance

An automatic universal testing machine (UTM4104X, SUNS, China) was utilized to measure the tensile strength (TS) and elongation at break (EAB) of the films, where the

starting clamping distance was fixed to 40 mm and the testing speed was set to 1 mm/s. Before testing, film strips (50 mm × 10 mm) were prepared, and their thickness was evaluated by a Mitutoyo digital micrometer (± 0.001 mm).

2.6.3. Thermogravimetric (TG) and differential scanning calorimetry (DSC) analysis

The thermostability of 6.0 mg film samples was analyzed using a TG analyzer (TGDTA7300, Hitachi, Japan) under nitrogen flow (50 mL/min). Samples were heated to 600 °C from 40 °C at the rate of 10 °C/min, and both curves of TG and derivative thermogravimetric (DTG) were recorded. The melting and crystallization behaviors of the films were further examined using differential scanning calorimetry (DSC 214 Polyma, NETZSCH, Germany). Approximately 2.0 mg of each film sample was placed in an aluminum pan and subjected to a heating–cooling–reheating cycle from 30 °C to 180 °C at a heating/cooling rate of 10 °C/min under a nitrogen atmosphere.

2.6.4. Water contact angle (WCA)

A video optical contact angle goniometer (JC2000C1, Shanghai Zhongchen Digital Technology Instruments Co., Ltd.) was utilized to evaluate the hydrophobic and hydrophilic properties of the film surfaces. The samples were mounted on slides, followed by carefully applying a droplet of water to the surface with a microsyringe. High-speed cameras were used to capture the images of the droplet, and the droplet contour data were analyzed using the Laplace-Young equation.

2.6.5. Water vapor transmission rate (WVTR)

The water vapor transmission rate (WVTR) of the film samples was measured with a water vapor transmission rate tester (W3/031, Labthink Instruments Co., Ltd., China). Circular films of 80 mm diameter were prepared and mounted onto permeation cells, with three replicate samples for each film. After preheating the instrument, measurements were conducted at 38.0 °C and 90% RH.

2.6.6. Water solubility (WS)

The films (20 mm × 40 mm) were dried at 40 °C to constant weight (m_1) and then immersed in distilled water (10 mL) for 24 h. They were dried again to constant weight (m_2). WS (%) was determined using equation (1).

$$WS = \frac{m_1 - m_2}{m_2} \quad (1)$$

2.6.7. Essential oil release behavior

A 10% ethanol (v/v) solution was utilized as the simulated medium, and films measuring 20 mm × 40 mm were immersed in 10 mL of solution. At specified time intervals, the absorbance of the solution at 278 nm was monitored to quantify the release of GEO from the film until equilibrium was achieved. Additionally, the release data were fitted to three differing models: Zero-order (2), Higuchi (3), and Ritger-Peppas (4). The accuracy of model fitting was assessed according to the correlation coefficient (R^2) (Dong et al., 2024).

$$\frac{M_t}{M_\infty} = kt \quad (2)$$

$$\frac{M_t}{M_\infty} = kt^{1/2} \quad (3)$$

$$\frac{M_t}{M_\infty} = kt^n \quad (4)$$

Where M_t represents the GEO release rate at time t, M_∞ denotes the GEO release rate at equilibrium, k is the release rate constant and n is the release exponent.

2.6.8. Antioxidant properties

The film samples (40 mm × 40 mm) were immersed in 4 mL of 0.1 mM DPPH solution and 4 mL of ABTS working solution, respectively, and allowed to react for 0.5 h in the dark. The absorbance was then measured at 517 nm (DPPH) and 734 nm (ABTS). Prior

to testing, the ABTS working solution was prepared following the report of Liu et al. (2024). Scavenging activities were calculated using Equation (5).

$$Scavenging\ rate(\%) = \frac{A_0 - A_1}{A_0} \times 100 \qquad (5)$$

In this equation, A_0 stands for the original absorbance of DPPH solution or ABTS working solution, and A_1 is the absorbance of solution after reaction with the film.

2.6.9. Antibacterial properties

The antibacterial activity of the films was evaluated using a disc diffusion assay following the method described by Hasheminya et al. (2019). *S. aureus* and *B. subtilis* (Gram-positive), as well as *E. coli* and *P. aeruginosa* (Gram-negative), were selected as representative bacteria. Briefly, a bacterial suspension (1.5×10^8 CFU/mL) was evenly spread onto a Mueller-Hinton agar plate using a throat swab. Then, 20 mm diameter circular film samples, sterilized by UV light, were placed on the agar surface. The inhibition zone diameter was estimated after the plates were incubated at 37 °C for 24 h.

2.7. Freshness preservation applications for composite films

The preservation experiment used fresh strawberries with uniform size and similar ripeness. The strawberries were stored in polyethylene (PE) film and in films loaded with varying concentrations of GOPE, under identical storage conditions (20 ± 2 °C, 50% ± 5% RH), with unpacked strawberries serving as controls. Strawberries were monitored for total soluble solids, hardness, and weight loss, as detailed in Section 3 of the Supplementary Materials.

2.8. Statistical analysis

Data analysis was performed using SPSS statistical software version 22.0 (SPSS Inc., Chicago, USA). Waller-Duncan's multiple range test was employed to assess mean

value differences, with a significance threshold set at $p < 0.05$.

3. Results and discussion

3.1. Characterization of ZTGs

Zein-TA-GA ternary nanoparticles (ZTGs) were prepared following the procedure outlined in Fig. 1A. The resulting ZTGs formed a homogeneous suspension with the average particle size of 234.27 ± 4.42 nm, a zeta potential of -22.70 ± 1.19 mV, and the polydispersity index (PDI) of 0.299 ± 0.012 (Fig. 1B). Fluorescence spectra (Fig. 1C) indicated the strongest fluorescence emission peak of zein nanoparticles at 304 nm, attributed to the high content of tyrosine residues in their structure (Yang et al., 2024b). Upon combining with tannic acid and gum Arabic, a red shift and a noticeable quenching of fluorescence intensity in the emission peak were observed. These changes suggest that zein interacts with tannic acid and gum Arabic, modifying the microenvironment surrounding the tyrosine residues (Liu et al., 2022). Fourier-transform infrared (FTIR) spectra (Fig. 1D) exhibited the characteristic peaks for zein at 3292 cm^{-1} (–OH stretching vibration), 1643 cm^{-1} (C=O stretching vibration, amide I), 1530 cm^{-1} (N-H bending vibration and C-N stretching vibration, amide II), and 1448 cm^{-1} ($–CH_2$ bending vibration). Upon the formation of ZTGs, the peak at 3292 cm^{-1} shifted to 3284 cm^{-1}, suggesting the generation of hydrogen bonds between the amide groups of zein and the phenolic hydroxyl groups in tannic acid, as well as the oxygen-containing functional groups in gum Arabic (Li et al., 2023b; Yang et al., 2024c). Additionally, slight shifts in the amide I and II bands were noticed, with peaks shifting to 1647 cm^{-1} and 1538 cm^{-1}, respectively, suggesting the involvement of electrostatic interactions in the formation of ZTGs (Li et al., 2023a). These electrostatic interactions are considered the primary driving force for the positively charged zein nanoparticles to bind to the anionic polysaccharide gum Arabic (Dai et al., 2018). Related studies have shown that zein nanoparticles are nearly spherical with a smooth surface (Zhou et al., 2024). However, SEM imaging observed that the surface of ZTGs was rough, with an irregular shape and adhesion between particles (Fig. 1E). These observations further

confirmed that zein successfully combined with tannic acid and gum Arabic and formed stable nanoparticles. Similar findings have been observed in other work (Liu et al., 2022; Zhang et al., 2024b). Additionally, the three-phase contact angle ($\theta_{o/w}$) of ZTGs (Fig. 1F) was measured at 94.15 ± 0.35°, indicating moderate wettability. This was a significant improvement over the wettability of zein nanoparticles alone ($\theta_{o/w}$ = 123.75 ± 0.25°), suggesting that the incorporation of tannic acid and gum Arabic enhanced the capability of nanoparticles to adsorb at the water-oil interface. These results indicated that ZTGs can effectively serve as emulsifiers for stabilizing Pickering emulsions.

3.2. Characterization of GOPE

GOPE with varying oil volume fractions (φ) was prepared. Optical microscopy images (Fig. 2A) indicated that as φ increased, the oil droplets' size also increased. This can be caused by the fact that the same area of the water-oil interface can be stabilized by the same concentration of nanoparticles. In emulsion systems with higher oil fractions, the only way to achieve an equivalent interface area is by enlarging the size of oil droplets (Wu et al., 2022). Quantitative analysis of droplet size further supported these observations. As shown in Fig. 2B, the surface mean diameter ($D_{3,2}$) of the GOPE droplets increased from 9.41 ± 0.41 μm at φ = 0.3 to 89.34 ± 14.41 μm at φ = 0.6, while the volume mean diameter ($D_{4,3}$) increased from 21.19 ± 2.16 μm to 160.61 ± 3.34 μm over the same φ range. Notably, at φ = 0.6, the droplet size increased sharply and droplet aggregation was observed, likely due to an insufficient number of nanoparticles to fully cover the water-oil interface. This indicates that φ = 0.6 represents a critical threshold for the stability of GOPE. As expected, the GOPE at φ = 0.75 rapidly demulsified after preparation, a phenomenon also observed under an optical microscope (Fig. 2A).

Interestingly, it was observed that GOPE with φ = 0.4, 0.5, and 0.6 transformed from emulsions to self-supporting emulsion gels on the first day of storage (Fig. 2C), indicating their potential for long-term storage stability (Xiao et al., 2024). Over the 60-day storage period, the GOPE with φ = 0.3 and 0.4 exhibited partial aqueous phase separation, while the GOPE with φ = 0.5 remained largely stable, with minimal phase

separation. To further assess the properties of the GOPE, rheological analysis was performed using both steady shear and dynamic oscillatory tests. As shown in Fig. 2D, all Pickering emulsions demonstrated typical shear-thinning behavior, in which the apparent viscosity decreased with increasing shear rate. This behavior is associated with the progressive disruption of the internal emulsion structure under shear, leading to the breakdown of droplet flocs and reduced resistance to flow (Wu et al., 2022). In contrast, the apparent viscosity increased with φ, likely because larger droplet sizes reduced the inter-droplet spacing, resulting in closer packing and stronger interactions that contributed to higher viscosity (Xu et al., 2023b).

Dynamic oscillatory scan results (Fig. 2E) showed that the loss modulus (G″) was consistently lower than the storage modulus (G′) across the entire range of frequency for all GOPE, except for the GOPE with φ = 0.3, validating the presence of a gel-like structure (Dai et al., 2019). Notably, GOPE with φ = 0.5 exhibited the highest values of both G′ and G″, suggesting the formation of a mechanically stronger emulsion gel. This enhanced viscoelastic behavior can be attributed to an optimal balance between the oil–water interfacial area and particle availability. At this φ, particles efficiently adsorb at the oil–water interface to form a compact and stable interfacial layer. Meanwhile, the close packing of particle-stabilized droplets promotes the formation of a continuous three-dimensional network across the system (Li et al., 2018a). The interface structure of the GOPE with φ = 0.5 was further analyzed with confocal laser scanning microscopy (CLSM). As exhibited in Fig. 2G, the green and red fluorescence signals represent the oil phase (GEO) and nanoparticles (ZTGs), respectively. The yellow fluorescence overlay indicates the stacking morphology of the oil phase and nanoparticles. It is evident that the GEO is densely encapsulated by the ZTGs, and this interfacial structure likely contributes to the long-term stability of GOPE (Wang et al., 2016). Additionally, the CLSM results confirm that GOPE is a typical O/W emulsion, a conclusion supported by the water phase dispersion method (Fig. 2F).

3.3. Identification of composite films

3.3.1. Visual appearance and optical properties

The UV-blocking capacity of packaging materials is crucial for protecting food from light-induced deterioration (Roy et al., 2024). Fig. 3A presents the UV-visible transmittance spectra of the films. It was observed that the incorporation of GOPE significantly blocked light in the UVA, UVB, and UVC regions. This improvement can be attributed to the synergistic effects of light scattering by GOPE droplets and light absorption by phenolic compounds or other chromophores in GEO (Zhang et al., 2024c). Moreover, food packaging materials with high transparency and colorless properties are often preferred by consumers, as they allow for better visual assessment of the food's original appearance and freshness (Guzman-Puyol et al., 2022). The color parameters of the films are exhibited in Fig. 3B. With the addition of GOPE, the films shifted toward red-yellow hues and exhibited a reduction in brightness, as indicated by an enhancement in the a* and b* values and a reduction in the L* value. However, from a visual perspective (Fig. 3C), the films containing GOPE still maintained relatively high transparency and near-colorless characteristics, which is crucial for their application in food packaging.

3.3.2. Structural characterization

The interactions between GOPE and the film matrix were first investigated by FTIR spectroscopy. Fig. 3D shows that all films exhibit broad and intense bands in the 3600-3000 cm^{-1} range, corresponding to the stretching vibrations of both intermolecular and intramolecular hydroxyl groups (Liu et al., 2020). A weak band observed in the 2990-2880 cm^{-1} range can be caused by the C-H stretching vibrations of CH_2 and CH_3 groups, while the peak at 1040 cm^{-1} is linked to the C-O-C stretching vibrations in the pyranose rings of sodium alginate and xylan (Liu et al., 2019b; Naidu & John, 2021). Moreover, the peak at 850 cm^{-1} is correlated to the C-O stretching vibrations in the glycosidic bonds of polysaccharides (Silva et al., 2024). Upon incorporation of GOPE, new absorption peaks appeared at 2860 cm^{-1} and 1740 cm^{-1}, which are attributed to the symmetric and asymmetric stretching vibrations of hydrophobic groups (CH_3, CH_2, and

CH) as well as the C=O stretching vibration in GEO (Chen et al., 2024; Xu et al., 2023a; Dai et al., 2023). The presence of these peaks confirms that GOPE was successfully integrated into the film matrix (Wang et al., 2024a). In addition, the shifts of the characteristic peaks from 3260 cm^{-1} to 3390 cm^{-1} and from 1600 cm^{-1} to 1650 cm^{-1}, accompanied by decreased signal intensity, indicate the formation of hydrogen bonding interactions between GOPE and the film matrix (Oun et al., 2022; Wang et al., 2023b). XRD was employed to characterize the crystalline structure of the films. As exhibited in Fig. 3E, the XL/SA/PVA film did not exhibit distinct characteristic diffraction peaks, indicating a predominantly amorphous structure (Wang et al., 2024a). The incorporation of GOPE did not markedly alter the diffraction peak positions, but it enhanced the intensity of the peak at $2\theta = 19.3°$, suggesting partial promotion of crystalline regions within the film matrix (Zhang et al., 2024a). This effect may be attributed to hydrogen-bonding interactions between GOPE and the film matrix, which enhance molecular contacts, reduce intermolecular spacing, and restrict molecular mobility, thereby facilitating the further development of crystalline regions (Cheng et al., 2024). Such changes in crystallinity are expected to influence the mechanical properties, water resistance, and thermostability of the films (Liu et al., 2024; Yang et al., 2024a).

To further elucidate the intermolecular interactions within the film matrix, molecular docking simulations were performed to analyze the interactions among xylan, sodium alginate, and PVA. The docking results (Fig. 3F) revealed multiple hydrogen bonding interactions among these components, indicating that hydrogen bonding plays a dominant role in stabilizing the polymer network and driving the film formation process.

3.3.3. Microstructure and topography

Fig. 4 presents the surface and cross-sectional microstructures of the films, along with three-dimensional surface morphology. The results showed that the XL/SA/PVA film exhibited a smooth surface with no obvious porosity, and its cross-sectional structure was dense and continuous, indicating good compatibility among the film-forming

components. In contrast, as the GOPE concentration increased, the film surface exhibited protrusions and micropores, as evidenced by an increase in the Ra value. Correspondingly, pores began to appear in the cross-section. During the film drying process, solvent evaporation caused emulsion droplets or aggregates to migrate toward the film surface, influenced by concentration and surface tension gradients. Some emulsion droplets may have evaporated with the solvent, leading to a non-homogeneous morphology on the film surface. Similar phenomena were observed in films based on other biopolymer matrices when Pickering emulsions were incorporated (Wang et al., 2023b; Wei et al., 2024; Wu et al., 2023). It is worth noting that the pore structure in the cross-section disrupted the compactness of the film matrix, which could directly weaken the mechanical characteristics of the film (Xu et al., 2023a), as validated in Section 3.3.4.

3.3.4. Thickness and mechanical characteristics

The tear resistance and deformation ability of films under external stresses are reflected by the tensile strength (TS) and the elongation at break (EAB), making them critical for assessing the practical applicability of films. As demonstrated in Fig. 5A, the XL/SA/PVA film showed the highest TS and EAB values, measuring 15.29 ± 1.16 MPa and 77.70 ± 14.53%, respectively. Upon incorporation of GOPE, both TS and EAB decreased ($P < 0.05$). At a GOPE concentration of 2%, the values of TS and EAB dropped to 7.65 ± 0.50 MPa and 47.71 ± 2.83%, respectively. SEM cross-sectional images clearly demonstrated that GOPE disrupted the compact internal structure of the film, weakening the matrix's cohesion and contributing to the reduction in TS (Yang et al., 2024d). Meanwhile, the XRD analysis indicates that the addition of GOPE promoted local ordering of polymer chains within the film matrix, thereby restricting chain mobility, which contributes to the decrease in EAB (Wang et al., 2020a). Accordingly, the deterioration in mechanical performance can be attributed to the combined effects of microstructural disruption at the macroscopic level and molecular-level constraints on polymer chain mobility. Notably, although enhanced local ordering

of polymer chains is generally associated with increased stiffness or TS, no such improvement was observed in the GOPE-containing films. This discrepancy suggests that the formation of microstructural defects, such as voids or discontinuities induced by GOPE incorporation, may play a more dominant role in governing the mechanical behavior of the films. Similar phenomena have also been reported by Xu et al. (2023a). In addition, the influence of film thickness on mechanical properties should also be considered. As shown in Fig. 5B, the film thickness gradually increased with increasing GOPE content. In principle, an increase in thickness can enhance structural compactness and mechanical strength by improving stress distribution (Yang et al., 2024e). However, the increase in thickness was primarily caused by the incorporation of GOPE, leading to surface protrusions and a more porous internal structure. Such microstructural defects and matrix discontinuity tended to offset potential reinforcing effect of increased thickness on the mechanical properties of the films. Fig. 5C presents images of the film containing 2% GOPE under various deformations and load-bearing conditions. Despite the reduced mechanical properties, the film still exhibited good flexibility and load-bearing capacity. This indicates that the active film has potential for practical applications, as it can effectively withstand external stresses encountered during packaging, transportation, and storage, while maintaining its integrity.

3.3.5. Thermostability

TG analysis (Fig. 5D) reveals that the films exhibit three main stages of weight loss. The initial weight loss was detected between 40 °C and 90 °C, which was associated with the evaporation of residual moisture within the film matrix. A second weight-loss stage was observed between 120 °C and 210 °C, primarily attributed to the degradation of glycerol (Liu et al., 2020). As the temperature continued to rise, the thermal decomposition of polymers such as xylan, sodium alginate, and PVA occurred, resulting in a third weight loss found from 230 °C to 280 °C (Liu et al., 2019b). Interestingly, films containing GOPE exhibited an additional weight-loss stage between 380 °C and 460 °C. Similar results were also stated by Yao et al. (2023) and Bu et al.

(2022b), who attributed this weight-loss stage to the existence of Pickering emulsions. Additionally, the films with GOPE exhibited higher residual mass from 230 °C to 280 °C as GOPE concentration increased, indicating that GOPE incorporation slows the thermal degradation of the film matrix. DTG analysis (Fig. 5E) revealed that the control film had a maximum thermal degradation temperature (T_{max}) of 269 °C. Upon incorporating GOPE, the T_{max} of the films progressively increased to 277 °C. These findings indicate that the added GOPE enhances the thermostability of the films. The DSC results further support this conclusion. As shown in Fig. 5F, the glass transition temperature (T_g) of the films increased progressively from 64.5 °C to 85.1 °C with increasing GOPE content. The elevation of T_g suggests enhanced structural rigidity and restricted molecular mobility within the polymer matrix, which is commonly associated with the reinforcement of ordered or crystalline-related regions, thereby requiring higher thermal energy for the transition from the glassy to rubbery state (Wang et al., 2023b). This trend is consistent with the crystalline-related features observed in the XRD analysis.

3.3.6. Water resistance properties

Water vapor transmission rate (WVTR) is a key indicator of moisture transfer efficiency across the film. A lower WVTR signifies enhanced water barrier characteristics, which help keep the moisture content, flavor, and texture of food products (Long et al., 2023). As illustrated in Fig. 5G, the films' WVTR markedly decreased ($P < 0.05$) from 1058.03 ± 72.25 g·cm^{-2}·24h^{-1} to 901.40 ± 44.95 g·cm^{-2}·24h^{-1} as GOPE concentrations increased, demonstrating notably improved water vapor barrier properties. Additionally, the incorporation of GOPE led to a decreased solubility of the films after 24-h immersion in water, reducing from 63.68% to 55.41% ($P < 0.05$) (Fig. 5H). These enhancements can be attributed to the hydrogen bonding interactions between the GOPE and the film matrix, which reduce the availability of hydrophilic groups (Liu et al., 2020). Furthermore, Bu et al. (2022a) highlighted that the increase in the films' crystallinity is a crucial factor contributing to enhanced water resistance.

This ordered molecular structure decreases the number of voids and channels for water molecules, limiting their interaction with the film matrix, and ultimately reducing the WVTR and solubility of the films.

The surface wettability of the films was further evaluated using static water contact angle (WCA) measurements. A contact angle of 65° is typically used as the threshold to distinguish hydrophilic from hydrophobic surfaces (Zhang et al., 2024a). As demonstrated in Fig. 5J, the XL/SA/PVA film exhibits a low WCA of 38.57°, indicating strong hydrophilicity. With increasing GOPE content, the WCA increased significantly, and the film surface transitioned from hydrophilic to hydrophobic at a GOPE concentration of 1%. This increase in WCA may be attributed to the preferential migration of GOPE toward the film–air interface during the drying process, leading to the enrichment and exposure of hydrophobic domains on the outer surface. Furthermore, the incorporation of GOPE enhances the intermolecular interactions within the film matrix, which may restrict the outward orientation and surface availability of hydrophilic functional groups (Wang et al., 2025).

3.3.7. Release kinetics of GEO from films

A 10% ethanol aqueous solution was selected as the simulated medium to investigate the release characteristics of GEO from films. According to Fig. 6A, GEO initially underwent a rapid release phase and then reached a steady state after a gradual slowdown. Additionally, the release rate of GEO reduced as the GOPE concentration increased. Xu et al. (2019) attributed this phenomenon to a decreased mass transfer concentration gradient.

To better understand the GEO' release behavior from the films, the release mechanism was explained using the Zero-order, Higuchi, and Ritger-Peppas kinetic models. Among these models, the Ritger-Peppas model exhibited the best fit, with regression coefficients (R^2) ranging from 0.9860 to 0.9940. The diffusion exponent (n) in the Ritger-Peppas model ($Mt/M\infty = kt^n$) indicates the type of diffusion mechanism. The

release follows Fickian diffusion when $n < 0.43$, primarily driven by the gradient of concentration. The release follows non-Fickian diffusion for $0.43 < n < 0.85$, involving a synergistic effect of concentration gradient and polymer swelling. When $n > 0.85$, diffusion is predominantly controlled by polymer swelling (Ran et al., 2023). As shown in Fig. 6D, all films exhibit n values below 0.43, indicating that GEO release is governed by a Fickian diffusion mechanism. Such diffusion-controlled release is advantageous for food packaging applications, as it allows a gradual release of active compounds and may contribute to sustained antimicrobial and antioxidant activity (Liang et al., 2024).

3.3.8 Antioxidant and antimicrobial characteristics

Phenolic compounds and unsaturated fatty acids present in food are highly susceptible to oxidation when exposed to oxygen or light, leading to free radical formation and subsequent deterioration reactions (Geng et al., 2023). In this study, DPPH and ABTS radical scavenging assays were employed to evaluate the antioxidant performance of the films. As shown in Fig. 7A and 7B, the incorporation of GOPE significantly enhances the free radical scavenging activities of the films ($P < 0.05$). Among these, the film containing 2.0% GOPE exhibits the highest antioxidant capacity, with DPPH and ABTS scavenging rates of 69.42 ± 2.19% and 93.85 ± 0.19%, respectively. Previous studies have reported that terpene compounds including α-zingiberene, α-curcumene, α-farnesene, α-sabinene, β-myrcene, β-sesquiphellandrene, β-bisabolene, and D-limonene in GEO can act as hydrogen or electron donors to neutralize free radicals (Badrunanto et al., 2024). These compounds are likely the primary contributors to the enhanced antioxidant activity observed in the films. Additionally, the tannic acid present in GOPE also contributes to the antioxidant activity, with the abundant phenolic hydroxyl groups on its benzene ring serving as the reaction sites for free radicals (Pourmadadi et al., 2024).

The antibacterial activity of films with varying GOPE concentrations was assessed using disk diffusion assay. The tested bacteria included foodborne pathogens (*S. aureus*

and *E. coli*) and spoilage bacteria (*P. aeruginosa* and *B. subtilis*). Because of the high hydrophilicity of XL/SA/PVA films without GOPE, they tended to curl and failed to spread uniformly on the MH agar medium, making evaluation impossible (results not shown). As shown in Fig. 7C and 7D, the GOPE-containing films exhibited antibacterial activity against all tested bacteria, demonstrating a concentration-dependent effect. In particular, the films containing 1.5% and 2.0% GOPE displayed more pronounced inhibition zones. A study by Al-Dhahli et al. (2020) revealed that α-curcumene and α-zingiberene have a higher affinity for bacterial proteins than other compounds in GEO, making them key contributors to its antibacterial activity. As GEO is gradually released from the film matrix, these bioactive compounds can disrupt the bacterial outer membrane, induce the leakage of intracellular component, and ultimately lead to cell death (Wang et al., 2020b).

3.4. Utilization of films for strawberry preservation

The preservation effectiveness of the films was evaluated by monitoring changes in visual appearance, firmness, weight loss, and soluble solids content of strawberries during storage. As shown in Fig. 8A, the decay regions of strawberries are highlighted with bold circles to facilitate direct visual comparison among different packaging groups. By the third day of storage, strawberries in the unpackaged group, as well as those wrapped in commercial PE film and XL/SA/PVA film, exhibited slight signs of decay. In contrast, no obvious decay was observed in strawberries packaged with GOPE-containing films at this stage. By the fifth day of storage, decay was observed in all groups except those packaged with films containing 1.5% and 2.0% GOPE, indicating a clear concentration-dependent preservation effect of GOPE. The weight loss behavior of strawberries during storage is presented in Fig. 8B. Unpackaged strawberries exhibited the highest weight loss throughout the storage period, which can be attributed to continuous water evaporation driven by respiration and transpiration processes (Li et al., 2024a). Strawberries wrapped in XL/SA/PVA-based films showed progressively lower weight loss with increasing GOPE content, which is consistent with

the reduced WVTR of the films, as discussed in Section 3.3.6. In contrast, strawberries packaged with commercial PE film displayed the lowest weight loss due to its superior water vapor barrier properties, which is in agreement with previous reports (Nong et al., 2025). However, despite the lower weight loss, the high-humidity microenvironment created by PE packaging may favor microbial growth, which helps explain the occurrence of decay observed in Fig. 8A (Zhang et al., 2023). Fig. 8C and Fig. 8D show the firmness and soluble solids content of strawberries after five days of storage. Compared with their initial values, all groups exhibited significant reductions in firmness and soluble solids content ($P < 0.05$), reflecting the natural progression of fruit senescence during storage. Notably, strawberries packaged with films containing 1.5% and 2.0% GOPE showed significantly smaller decreases in both parameters. This can be attributed to the enhanced antioxidant and antimicrobial activities of the films at higher GOPE concentrations (Fig. 7), which effectively delayed oxidative deterioration, inhibited microbial proliferation, and slowed metabolic processes related to fruit softening and nutrient depletion. Consequently, higher firmness and soluble solids content were retained.

4. Conclusion

In this work, ternary nanoparticles composed of zein, tannic acid, and gum Arabic (ZTGs) were successfully constructed and exhibited an average particle size of 234.27 ± 4.42 nm and a three-phase contact angle of 94.15 ± 0.35°, indicating near- medium wettability and favorable characteristics for Pickering emulsion stabilization. GOPE stabilized by ZTGs formed emulsion gels at oil phase volume fractions ranging from 0.4 to 0.6, with $\varphi = 0.5$ exhibiting the most favorable interfacial properties. The ZTGs-stabilized GOPE showed high compatibility with the XL/SA/PVA film-forming matrix, where hydrogen bonding was identified as the dominant interaction among components. The incorporation of GOPE increased the degree of crystallinity within the films, leading to enhanced thermostability and water resistance. However, the introduction of GOPE also disrupted the continuity of the polymer matrix, resulting in a reduction in

mechanical strength. Despite this trade-off, the films maintained sufficient flexibility and load-bearing capacity, suggesting their suitability for practical handling and packaging applications. Moreover, the incorporation of GOPE endowed the films with both antioxidant and antibacterial activities. When applied to strawberry preservation, films containing 1.5% and 2.0% GOPE effectively delayed fruit spoilage and maintained postharvest quality. Overall, these findings confirm the feasibility of employing ZTGs-stabilized Pickering emulsions as functional additives in bio-based active films and highlight their potential for food packaging applications. Nevertheless, further studies are needed to evaluate the long-term stability and release behavior of the films under various storage conditions, and to determine whether the incorporation of GOPE affects fruit aroma and sensory attributes, which is crucial for practical food packaging applications.

Declaration of competing interest

The authors declare no conflict of interest.

Acknowledgements

This research was supported by the *Key R&D* Project of Shandong Province (2023TZXD070)

References

Acharya, D. R., Liu, S., Lu, H., Albashir, D., Koirala, P., Shi, Y., & Chen, Q. (2024). Nanoemulsion-integrated gelatin/bacterial cellulose nanofibril-based multifunctional film: Fabrication, characterization, and application. *International Journal of Biological Macromolecules*, *257*, 128341. https://doi.org/10.1016/j.ijbiomac.2023.128341

Al-Dhahli, A. S., Al-Hassani, F. A., Mohammed Alarjani, K., Mohamed Yehia, H., Al Lawati, W. M., Najmul Hejaz Azmi, S., & Alam Khan, S. (2020). Essential oil from the rhizomes of the Saudi and Chinese *Zingiber officinale* cultivars: Comparison of chemical composition, antibacterial and molecular docking

studies. *Journal of King Saud University - Science*, *32*(8), 3343-3350. https://doi.org/10.1016/j.jksus.2020.09.020

Badrunanto, Wahyuni, W. T., Farid, M., Batubara, I., & Yamauchi, K. (2024). Antioxidant components of the three different varieties of Indonesian ginger essential oil: *In vitro* and computational studies. *Food Chemistry Advances*, *4*, 100558. https://doi.org/10.1016/j.focha.2023.100558

Bu, N., Huang, L., Cao, G., Lin, H., Pang, J., Wang, L., & Mu, R. (2022a). Konjac glucomannan/Pullulan films incorporated with cellulose nanofibrils-stabilized tea tree essential oil Pickering emulsions. *Colloids and Surfaces A: Physicochemical and Engineering Aspects*, *650*, 129553. https://doi.org/10.1016/j.colsurfa.2022.129553

Bu, N., Sun, R., Huang, L., Lin, H., Pang, J., Wang, L., & Mu, R. (2022b). Chitosan films with tunable droplet size of Pickering emulsions stabilized by amphiphilic konjac glucomannan network. *International Journal of Biological Macromolecules*, *220*, 1072-1083. https://doi.org/10.1016/j.ijbiomac.2022.08.157

Cao, Y., Yin, L., Li, F., Deng, Y., Kong, B., Liu, Q., Wang, H., & Wang, H. (2024). Characterization of sodium alginate film containing zein-Arabic gum nanoparticles encapsulated with oregano essential oil for chilled pork packaging. *International Journal of Biological Macromolecules*, *278*, 134824. https://doi.org/10.1016/j.ijbiomac.2024.134824

Chen, G., Fu, Y., Niu, F., Zhang, H., Li, X., & Li, X. (2019). Evaluation of the colloidal/chemical performance of core-shell nanoparticle formed by zein and gum Arabic. *Colloids and Surfaces A: Physicochemical and Engineering Aspects*, *560*, 130-135. https://doi.org/10.1016/j.colsurfa.2018.10.006

Chen, X., Lan, W., & Xie, J. (2024). Characterization of active films based on chitosan/polyvinyl alcohol integrated with ginger essential oil-loaded bacterial cellulose and application in sea bass (*Lateolabrax japonicas*) packaging. *Food Chemistry*, *441*, 138343. https://doi.org/10.1016/j.foodchem.2023.138343

Cheng, M., Shu, Y., Li, M., Li, C., Liang, T., & Zhang, Z. (2024). Characterisation of

an edible active film prepared from bacterial nanocellulose/forsythia essential oil Pickering emulsions with funoran and its application in fresh meat. *International Journal of Biological Macromolecules, 280*, 136141. https://doi.org/10.1016/j.ijbiomac.2024.136141

Dai, H., Chen, Y., Chen, H., Fu, Y., Ma, L., Wang, H., Yu, Y., Zhu, H., & Zhang, Y. (2023). Gelatin films functionalized by lignocellulose nanocrystals-tannic acid stabilized Pickering emulsions: Influence of cinnamon essential oil. *Food Chemistry*, *401*, 134154. https://doi.org/10.1016/j.foodchem.2022.134154

Dai, L., Sun, C., Wei, Y., Mao, L., & Gao, Y. (2018). Characterization of Pickering emulsion gels stabilized by zein/gum arabic complex colloidal nanoparticles. *Food Hydrocolloids*, *74*, 239-248. https://doi.org/10.1016/j.foodhyd.2017.07.040

Dai, L., Yang, S., Wei, Y., Sun, C., McClements, D. J., Mao, L., & Gao, Y. (2019). Development of stable high internal phase emulsions by pickering stabilization: Utilization of zein-propylene glycol alginate-rhamnolipid complex particles as colloidal emulsifiers. *Food Chemistry*, *275*, 246-254. https://doi.org/10.1016/j.foodchem.2018.09.122

de Folter, J. W. J., van Ruijven, M. W. M., & Velikov, K. P. (2012). Oil-in-water Pickering emulsions stabilized by colloidal particles from the water-insoluble protein zein. *Soft Matter*, *8*(25), 6807-6815. https://doi.org/10.1039/C2SM07417F

Dong, J., Yu, D., Zhang, L., Wang, G., Zhang, P., You, Y., Xu, Y., & Xia, W. (2024). Chitosan/alginate dialdehyde trilayer films with cinnamaldehyde nanoemulsions for grass carp preservation. *Food Hydrocolloids*, *147*, 109413. https://doi.org/10.1016/j.foodhyd.2023.109413

Gali, L., Bedjou, F., Ferrari, G., & Donsì, F. (2022). Formulation and characterization of zein/gum arabic nanoparticles for the encapsulation of a rutin-rich extract from *Ruta chalepensis L*. *Food Chemistry*, *367*, 129982. https://doi.org/10.1016/j.foodchem.2021.129982

Geng, L., Liu, K., & Zhang, H. (2023). Lipid oxidation in foods and its implications on

proteins. *Frontiers in Nutrition*, *10*. https://doi.org/10.3389/fnut.2023.1192199

Guzman-Puyol, S., Benítez, J. J., & Heredia-Guerrero, J. A. (2022). Transparency of polymeric food packaging materials. *Food Research International*, *161*, 111792. https://doi.org/10.1016/j.foodres.2022.111792

Hasheminya, S.-M., Mokarram, R. R., Ghanbarzadeh, B., Hamishekar, H., Kafil, H. S., & Dehghannya, J. (2019). Influence of simultaneous application of copper oxide nanoparticles and *Satureja Khuzestanica* essential oil on properties of kefiran–carboxymethyl cellulose films. *Polymer Testing*, *73*, 377-388. https://doi.org/10.1016/j.polymertesting.2018.12.002

Jiang, Y., Wang, D., Li, F., Li, D., & Huang, Q. (2020). Cinnamon essential oil Pickering emulsion stabilized by zein-pectin composite nanoparticles: Characterization, antimicrobial effect and advantages in storage application. *International Journal of Biological Macromolecules*, *148*, 1280-1289. https://doi.org/10.1016/j.ijbiomac.2019.10.103

Jing, W., Xiaolan, C., Yu, C., Feng, Q., & Haifeng, Y. (2022). Pharmacological effects and mechanisms of tannic acid. *Biomedicine & Pharmacotherapy*, *154*, 113561. https://doi.org/10.1016/j.biopha.2022.113561

Kaur, G., & Mehta, S. K. (2017). Developments of Polysorbate (Tween) based microemulsions: Preclinical drug delivery, toxicity and antimicrobial applications. *International Journal of Pharmaceutics*, *529*(1), 134-160. https://doi.org/10.1016/j.ijpharm.2017.06.059

Li, J., Wang, Y., Ma, Y., Zheng, N., Liu, J., & Liu, T. (2024a). Preparation and characterization of chitosan-based corn protein composites constructed with TG enzyme and their preservation performance on strawberries. *International Journal of Biological Macromolecules*, *270*, 132190. https://doi.org/10.1016/j.ijbiomac.2024.132190

Li, J., Xu, X., Chen, Z., Wang, T., Lu, Z., Hu, W., & Wang, L. (2018a). Zein/gum Arabic nanoparticle-stabilized Pickering emulsion with thymol as an antibacterial delivery system. *Carbohydrate Polymers*, *200*, 416-426. https://doi.org/10.1016/j.carbpol.2018.08.025

Li, J., Xu, X., Chen, Z., Wang, T., Wang, L., & Zhong, Q. (2018b). Biological macromolecule delivery system fabricated using zein and gum arabic to control the release rate of encapsulated tocopherol during *in vitro* digestion. *Food Research International*, *114*, 251-257. https://doi.org/10.1016/j.foodres.2018.08.073

Li, R., Feng, H., Wang, S., Zhuang, D., Wen, Y., & Zhu, J. (2024b). A double-layer film based on the strategy of tannic acid-anthocyanin co-pigmentation and tannic-crosslinked-gelatin/−reduced Ag nanoparticles for beef preservation and monitoring. *Food Chemistry*, *460*, 140642. https://doi.org/10.1016/j.foodchem.2024.140642

Li, R., Zhang, Z., Chen, J., Li, H., & Tang, H. (2023a). Investigating of zein-gum arabic-tea polyphenols ternary complex nanoparticles for luteolin encapsulation: Fabrication, characterization, and functional performance. *International Journal of Biological Macromolecules*, *242*, 125059. https://doi.org/10.1016/j.ijbiomac.2023.125059

Li, S., Li, S., Gong, M., Zhang, H., Fan, L., Liu, X., & Zhou, J. (2023b). Development of Zein/tannic acid nanoparticles as antioxidants for oxidation inhibition of blackberry seed oil emulsions. *Food Chemistry*, *403*, 134236. https://doi.org/10.1016/j.foodchem.2022.134236

Liang, W., Ge, X., Lin, Q., Niu, L., Zhao, W., Muratkhan, M., & Li, W. (2024). Ternary composite degradable plastics based on *Alpinia galanga* essential oil Pickering emulsion templates: A potential multifunctional active packaging. *International Journal of Biological Macromolecules*, *257*, 128580. https://doi.org/10.1016/j.ijbiomac.2023.128580

Liang, X., Cao, K., Li, W., Li, X., McClements, D. J., & Hu, K. (2021). Tannic acid-fortified zein-pectin nanoparticles: Stability, properties, antioxidant activity, and *in vitro* digestion. *Food Research International*, *145*, 110425. https://doi.org/10.1016/j.foodres.2021.110425

Liu, J., Fauconnier, M.-L., Richel, A., & Jin, Y. (2024). Preparation of active films with antioxidant and antimicrobial properties by combining ginger essential oil

nanoemulsion with xylan and polyvinyl alcohol. *International Journal of Biological Macromolecules*, *281*, 135780. https://doi.org/10.1016/j.ijbiomac.2024.135780

Liu, Q.-R., Wang, W., Qi, J., Huang, Q., & Xiao, J. (2019a). Oregano essential oil loaded soybean polysaccharide films: Effect of Pickering type immobilization on physical and antimicrobial properties. *Food Hydrocolloids*, *87*, 165-172. https://doi.org/10.1016/j.foodhyd.2018.08.011

Liu, X., Chen, X., Ren, J., Chang, M., He, B., & Zhang, C. (2019b). Effects of nano-ZnO and nano-SiO_2 particles on properties of PVA/xylan composite films. *International Journal of Biological Macromolecules*, *132*, 978-986. https://doi.org/10.1016/j.ijbiomac.2019.03.088

Liu, X., Xie, F., Zhou, J., He, J., Din, Z.-u., Cheng, S., & Cai, J. (2023). High internal phase Pickering emulsion stabilized by zein-tannic acid-sodium alginate complexes: β-Carotene loading and 3D printing. *Food Hydrocolloids*, *142*, 108762. https://doi.org/10.1016/j.foodhyd.2023.108762

Liu, Y., Liang, Q., Liu, X., Raza, H., Ma, H., & Ren, X. (2022). Treatment with ultrasound improves the encapsulation efficiency of resveratrol in zein-gum Arabic complex coacervates. *LWT*, *153*, 112331. https://doi.org/10.1016/j.lwt.2021.112331

Liu, Z., Lin, D., Shen, R., & Yang, X. (2020). Characterizations of novel konjac glucomannan emulsion films incorporated with high internal phase Pickering emulsions. *Food Hydrocolloids*, *109*, 106088. https://doi.org/10.1016/j.foodhyd.2020.106088

Long, J., Zhang, W., Zhao, M., & Ruan, C.-Q. (2023). The reduce of water vapor permeability of polysaccharide-based films in food packaging: A comprehensive review. *Carbohydrate Polymers*, *321*, 121267. https://doi.org/10.1016/j.carbpol.2023.121267

Mutlu, N. (2023). Effects of grape seed oil nanoemulsion on physicochemical and antibacterial properties of gelatin-sodium alginate film blends. *International Journal of Biological Macromolecules*, *237*, 124207.

https://doi.org/10.1016/j.ijbiomac.2023.124207

Naidu, D. S., & John, M. J. (2021). Cellulose nanofibrils reinforced xylan-alginate composites: Mechanical, thermal and barrier properties. *International Journal of Biological Macromolecules*, *179*, 448-456. https://doi.org/10.1016/j.ijbiomac.2021.03.035

Najari, Z., Dokouhaki, M., Juliano, P., & Adhikari, B. (2024). Advances in the application of protein-polysaccharide-polyphenol ternary complexes for creating and stabilizing Pickering emulsions. *Future Foods*, *9*, 100299. https://doi.org/10.1016/j.fufo.2024.100299

Nong, W., Luo, H., Wang, G., Chen, Q., Zou, X., Miao, W., Wu, J., Guan, W., & Qu, S. (2025). β-CD-MOF-based edible antimicrobial packaging film with humidity-controlled carvacrol release for preserving fresh strawberry. *Carbohydrate Polymers*, *351*, 123133. https://doi.org/10.1016/j.carbpol.2024.123133

Oun, A. A., Shin, G. H., & Kim, J. T. (2022). Multifunctional poly(vinyl alcohol) films using cellulose nanocrystals/oregano and cellulose nanocrystals/cinnamon Pickering emulsions: Effect of oil type and concentration. *International Journal of Biological Macromolecules*, *194*, 736-745. https://doi.org/10.1016/j.ijbiomac.2021.11.119

Pérez-Córdoba, L. J., Norton, I. T., Batchelor, H. K., Gkatzionis, K., Spyropoulos, F., & Sobral, P. J. A. (2018). Physico-chemical, antimicrobial and antioxidant properties of gelatin-chitosan based films loaded with nanoemulsions encapsulating active compounds. *Food Hydrocolloids*, *79*, 544-559. https://doi.org/10.1016/j.foodhyd.2017.12.012

Pourmadadi, M., Omrani, Z., Abbasi, R., Mirshafiei, M., & Yazdian, F. (2024). Poly (Tannic Acid) based nanocomposite as a promising potential in biomedical applications. *Journal of Drug Delivery Science and Technology*, *95*, 105568. https://doi.org/10.1016/j.jddst.2024.105568

Ran, R., Zheng, T., Tang, P., Xiong, Y., Yang, C., Gu, M., & Li, G. (2023). Antioxidant and antimicrobial collagen films incorporating Pickering emulsions of cinnamon essential oil for pork preservation. *Food Chemistry*, *420*, 136108.

https://doi.org/10.1016/j.foodchem.2023.136108

Roy, S., Ramakrishnan, R., Goksen, G., Singh, S., & Łopusiewicz, Ł. (2024). Recent progress on UV-light barrier food packaging films – a systematic review. *Innovative Food Science & Emerging Technologies*, *91*, 103550. https://doi.org/10.1016/j.ifset.2023.103550

Silva, J. M., Vilela, C., Girão, A. V., Branco, P. C., Martins, J., Freire, M. G., Silvestre, A. J. D., & Freire, C. S. R. (2024). Wood inspired biobased nanocomposite films composed of xylans, lignosulfonates and cellulose nanofibers for active food packaging. *Carbohydrate Polymers*, *337*, 122112. https://doi.org/10.1016/j.carbpol.2024.122112

Wang, J.-D., Yang, S.-L., Liu, G.-S., Zhou, Q., Fu, L.-N., Gu, Q., Cai, Z.-H., Zhang, S., & Fu, Y.-J. (2024a). A degradable multi-functional packaging based on chitosan/silk fibroin via incorporating cellulose nanocrystals-stabilized cinnamon essential oil pickering emulsion. *Food Hydrocolloids*, *153*, 109978. https://doi.org/10.1016/j.foodhyd.2024.109978

Wang, J., Zhao, F., Huang, J., Li, Q., Yang, Q., & Ju, J. (2024b). Application of essential oils as slow-release antimicrobial agents in food preservation: Preparation strategies, release mechanisms and application cases. *Critical Reviews in Food Science and Nutrition*, *64*(18), 6272-6297. https://doi.org/10.1080/10408398.2023.2167066

Wang, L.-J., Yin, S.-W., Wu, L.-Y., Qi, J.-R., Guo, J., & Yang, X.-Q. (2016). Fabrication and characterization of Pickering emulsions and oil gels stabilized by highly charged zein/chitosan complex particles (ZCCPs). *Food Chemistry*, *213*, 462-469. https://doi.org/10.1016/j.foodchem.2016.06.119

Wang, L., Lin, L., Guo, Y., Long, J., Mu, R.-J., & Pang, J. (2020a). Enhanced functional properties of nanocomposite film incorporated with EGCG-loaded dialdehyde glucomannan/gelatin matrix for food packaging. *Food Hydrocolloids*, *108*, 105863. https://doi.org/10.1016/j.foodhyd.2020.105863

Wang, X., Shen, Y., Thakur, K., Han, J., Zhang, J.-G., Hu, F., & Wei, Z.-J. (2020b). Antibacterial activity and mechanism of ginger essential oil against *Escherichia*

coli and *Staphylococcus aureus*. *Molecules*, *25*(17), 3955. https://www.mdpi.com/1420-3049/25/17/3955

Wang, X., Li, S., Zeng, M., Gong, H., Zhang, Z., Yuan, X., Zhou, M., Chen, A., Liu, Y., & Wu, H. (2025). Preparation, characterization and application of antimicrobial pectin-konjac glucomannan composite films incorporating cellulose nanocrystals stabilized clove essential oil pickering emulsion. *LWT*, *225*, 117855. https://doi.org/10.1016/j.lwt.2025.117855

Wang, Y., Kratzer, R., Murkovic, M., Eibinger, M., Machado Charry, E., Li, S., Zhang, T., Zhang, X., Zhang, M., & Chen, H. (2023a). Fabrication and characterization of a novel zein/pectin/pumpkin seed oil Pickering emulsion and the effects of myricetin on oxidation stability. *International Journal of Biological Macromolecules*, *253*, 127386. https://doi.org/10.1016/j.ijbiomac.2023.127386

Wang, Y., Ni, X., Wen, M., Lou, S., Xiao, W., & Gao, Z. (2023b). Preparation of antioxidant konjac glucomannan-based films enriched with *Ocimum gratissimum* L. essential oil Pickering emulsion and its effect on walnuts preservation. *Colloids and Surfaces A: Physicochemical and Engineering Aspects*, *665*, 131220. https://doi.org/10.1016/j.colsurfa.2023.131220

Wei, L., Li, J., Qin, X., Wang, Q., & Zhong, J. (2024). Enhancing the antioxidant properties and compatibility of protein/sodium alginate film by incorporating *Zanthoxylum bungeanum* essential oil Pickering emulsion. *Food Chemistry*, *445*, 138771. https://doi.org/10.1016/j.foodchem.2024.138771

Wu, B., Zhang, S., Jiang, X., Hou, P., Xin, Y., Zhang, L., Zhang, J., & Zhou, D. (2022). Impact of weakly charged insoluble karaya gum on zein nanoparticle and mechanism for stabilizing Pickering emulsions. *International Journal of Biological Macromolecules*, *222*, 121-131. https://doi.org/10.1016/j.ijbiomac.2022.09.066

Wu, H., Wang, J., Li, T., Lei, Y., Peng, L., Chang, J., Li, S., Yuan, X., Zhou, M., & Zhang, Z. (2023). Effects of cinnamon essential oil-loaded Pickering emulsion on the structure, properties and application of chayote tuber starch-based composite films. *International Journal of Biological Macromolecules*, *240*,

124444. https://doi.org/10.1016/j.ijbiomac.2023.124444

Xiao, M., Li, S., Xiong, L., Duan, J., Chen, X., Luo, X., Wang, D., Zou, L., Li, J., Hu, Y., & Zhang, J. (2024). Pickering emulsion gel of polyunsaturated fatty acid-rich oils stabilized by zein-tannic acid green nanoparticles for storage and oxidation stability enhancement. *Journal of Colloid and Interface Science*, *675*, 646-659. https://doi.org/10.1016/j.jcis.2024.06.190

Xu, J., He, M., Wei, C., Duan, M., Yu, S., Li, D., Zhong, W., Tong, C., Pang, J., & Wu, C. (2023a). Konjac glucomannan films with Pickering emulsion stabilized by TEMPO-oxidized chitin nanocrystal for active food packaging. *Food Hydrocolloids*, *139*, 108539. https://doi.org/10.1016/j.foodhyd.2023.108539

Xu, T., Gao, C., Feng, X., Huang, M., Yang, Y., Shen, X., & Tang, X. (2019). Cinnamon and clove essential oils to improve physical, thermal and antimicrobial properties of chitosan-gum arabic polyelectrolyte complexed films. *Carbohydrate Polymers*, *217*, 116-125. https://doi.org/10.1016/j.carbpol.2019.03.084

Xu, X., Li, L., Ma, C., Li, D., Yang, Y., Bian, X., Fan, J., Zhang, N., & Zuo, F. (2023b). Soy protein isolate-citrus pectin-gallic acid ternary composite high internal phase Pickering emulsion for delivery of β-carotene: Physicochemical, structural and digestive properties. *Food Research International*, *169*, 112910. https://doi.org/10.1016/j.foodres.2023.112910

Yang, W., Zhang, S., Feng, A., Li, Y., Wu, P., Li, H., & Ai, S. (2024a). Water-insoluble tea polyphenol nanoparticles as fillers and bioactive agents for pectin films to prepare active packaging for fruit preservation. *Food Hydrocolloids*, *156*, 110364. https://doi.org/10.1016/j.foodhyd.2024.110364

Yang, X., Lv, Z., Han, C., Zhang, J., Duan, Y., & Guo, Q. (2024b). Stability and encapsulation properties of daidzein in zein/carrageenan/sodium alginate nanoparticles with ultrasound treatment. *International Journal of Biological Macromolecules*, *262*, 130070. https://doi.org/10.1016/j.ijbiomac.2024.130070

Yang, Y., Jia, Y., Zhang, M., Luo, Y., Zhang, Z., Wu, W., & Yuan, L. (2024c). Synthesis, characterization, antioxidant and bacteriostasis in preservation of isoorientin

loaded Zein/GA nanoparticles. *Food Chemistry: X*, *23*, 101604. https://doi.org/10.1016/j.fochx.2024.101604

Yang, Z., Chen, B., Tahir, H. E., Li, Z., Huang, X., Li, M., Zhang, K., Li, B., Zhai, X., Shi, J., Zou, X., & Xiao, J. (2024d). Gelatin/sodium alginate-based biodegradable films functionalized by persimmon pectin/ovalbumin-stabilized neem essential oil Pickering emulsion: Application for cherry tomato preservation. *Progress in Organic Coatings*, *192*, 108448. https://doi.org/10.1016/j.porgcoat.2024.108448

Yang, W., Zhang, S., Hu, Y., Fu, Q., Cheng, X., Li, Y., Wu, P., Li, H., & Ai, S. (2024e). Pectin-based film activated with carboxylated cellulose nanocrystals-stabilized oregano essential oil Pickering emulsion. *Food Hydrocolloids*, *151*, 109781. https://doi.org/10.1016/j.foodhyd.2024.109781

Yao, L., Man, T., Xiong, X., Wang, Y., Duan, X., & Xiong, X. (2023). HPMC films functionalized by zein/carboxymethyl tamarind gum stabilized Pickering emulsions: Influence of carboxymethylation degree. *International Journal of Biological Macromolecules*, *238*, 124053. https://doi.org/10.1016/j.ijbiomac.2023.124053

Zhang, S., Cheng, X., Fu, Q., Li, Y., Wu, P., Qiao, Y., Yan, J., Si, L., Waterhouse, G. I. N., Li, H., & Ai, S. (2023). Pectin-nanolignin composite films with water resistance, UV resistance, and antibacterial activity. *Food Hydrocolloids*, *143*, 108783. https://doi.org/10.1016/j.foodhyd.2023.108783

Zhang, S., Fu, Q., Li, H., Li, Y., Wu, P., & Ai, S. (2024a). Polydopamine-coated lignin nanoparticles in polysaccharide-based films: A plasticizer, mechanical property enhancer, anti-ultraviolet agent and bioactive agent. *Food Hydrocolloids*, *147*, 109325. https://doi.org/10.1016/j.foodhyd.2023.109325

Zhang, W., Huan, Y., Ren, P., Li, J., Wei, Z., Xu, J., & Tang, Q. (2024b). Zein/hyaluronic acid nanoparticle stabilized Pickering emulsion for astaxanthin encapsulation. *International Journal of Biological Macromolecules*, *255*, 127992. https://doi.org/10.1016/j.ijbiomac.2023.127992

Zhang, X., Liu, D., Jin, T. Z., Chen, W., He, Q., Zou, Z., Zhao, H., Ye, X., & Guo, M.

(2021). Preparation and characterization of gellan gum-chitosan polyelectrolyte complex films with the incorporation of thyme essential oil nanoemulsion. *Food Hydrocolloids*, *114*, 106570. https://doi.org/10.1016/j.foodhyd.2020.106570

Zhang, Y., Pu, Y., Jiang, H., Chen, L., Shen, C., Zhang, W., Cao, J., & Jiang, W. (2024c). Improved sustained-release properties of ginger essential oil in a Pickering emulsion system incorporated in sodium alginate film and delayed postharvest senescence of mango fruits. *Food Chemistry*, *435*, 137534. https://doi.org/10.1016/j.foodchem.2023.137534

Zhang, Y., Liu, G., Ren, F., Liu, N., Tong, Y., Li, Y., Liu, A., Wu, L., & Wang, P. (2022). Delivery of curcumin using zein-gum Arabic-tannic acid composite particles: fabrication, characterization, and *in vitro* release properties. *Frontiers in Nutrition*, *9* , 842850. https://doi.org/10.3389/fnut.2022.842850

Zhao, Q., Fan, L., Li, J., & Zhong, S. (2024). Pickering emulsions stabilized by biopolymer-based nanoparticles or hybrid particles for the development of food packaging films: A review. *Food Hydrocolloids*, *146*, 109185. https://doi.org/10.1016/j.foodhyd.2023.109185

Zhou, D., Xin, Y., Wu, B., Jiang, X., Wu, X., Hou, P., Qi, J., & Zhang, J. (2024). Pickering emulsions stabilized by ternary complexes involving curcumin-modified zein and polysaccharides with different charge amounts for encapsulating β-carotene. *Food Chemistry*, *433*, 137338. https://doi.org/10.1016/j.foodchem.2023.137338

All authors discussed the results and commented on the manuscript. No conflicts of interest were identified.

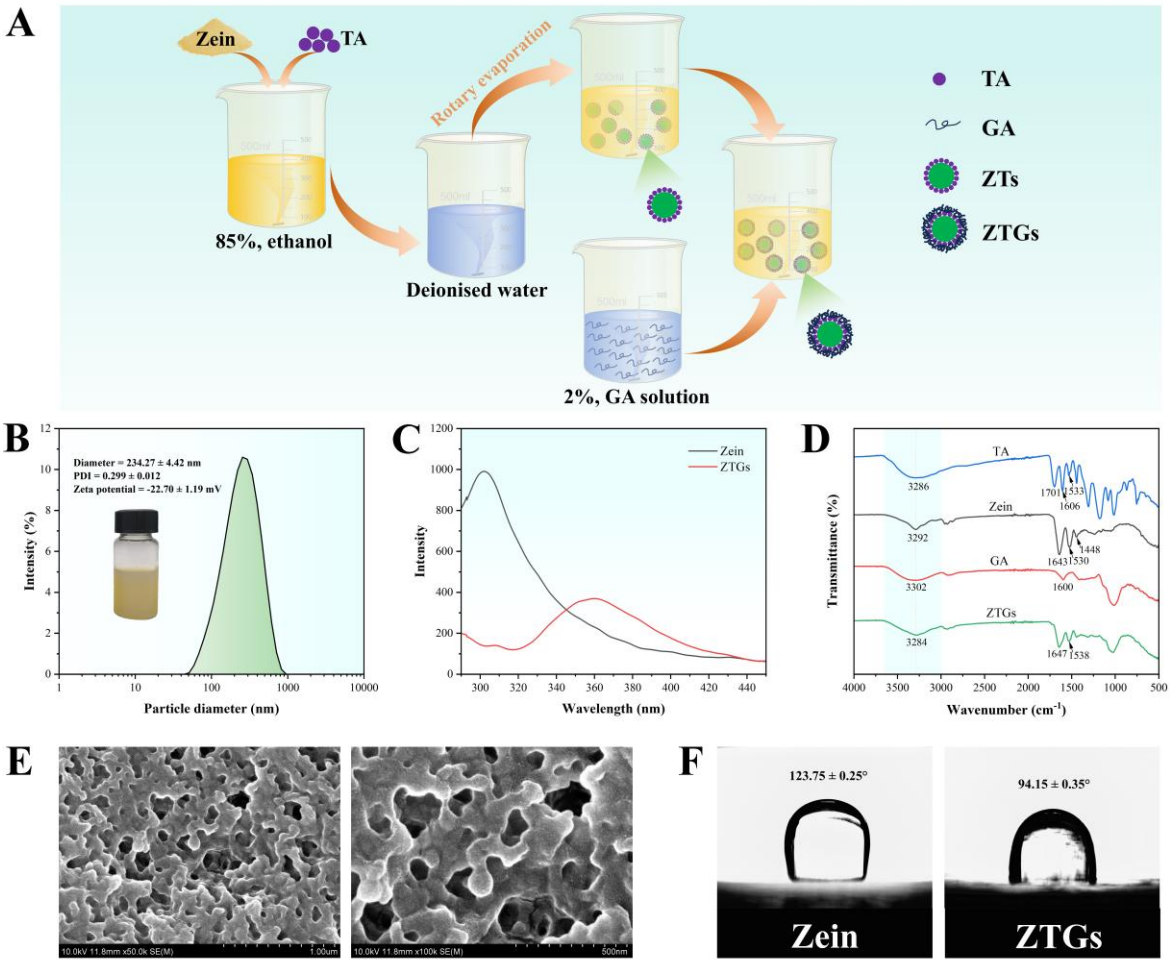

Fig. 1. Schematic illustration of the preparation process of zein–tannic acid–gum Arabic ternary nanoparticles (ZTGs) (A); Appearance, particle size, PDI and zeta potential of ZTGs (B); Fluorescence spectra of zein and ZTGs (C); FTIR spectra of zein, tannic acid (TA), gum Arabic (GA) and ZTGs (D); SEM images of ZTGs at ×50 k and ×100 k magnification (E); The three-phase contact angle of zein and ZTGs (F).

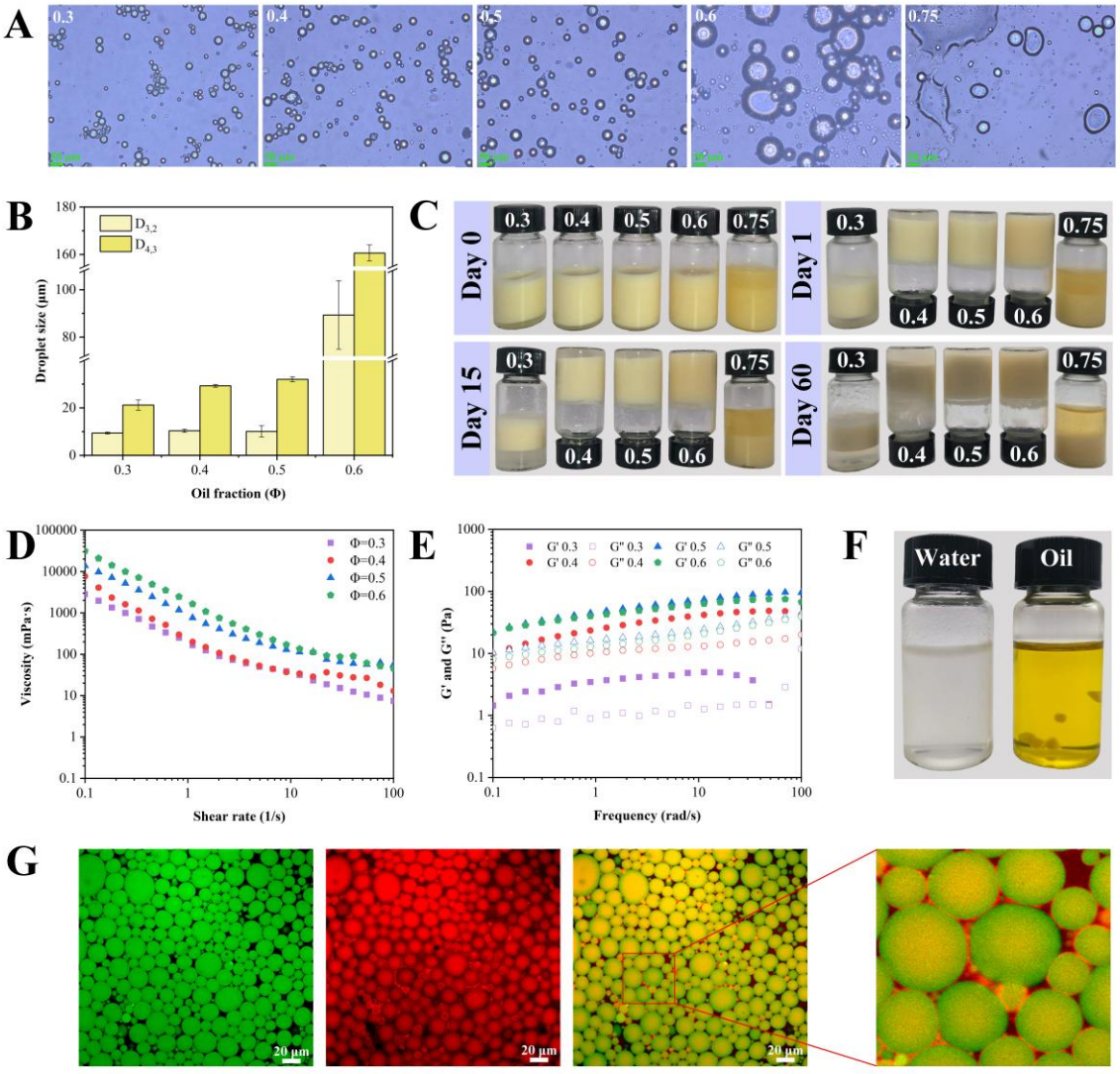

Fig. 2. Optical microscopic images (A), droplet size ($D_{3,2}$ and $D_{4,3}$) (B), visual appearance photograph (storage for 0, 1, 15 and 60 days, respectively) (C), and rheological properties (G′: storage modulus, G″: loss modulus) (D,E) of ginger essential oil Pickering emulsions (GOPE) with

various oil fractions (φ = 0.3, 0.4, 0.5, 0.6, and 0.75); Dispersion of emulsion gel droplets in deionized water and oil (F); Confocal laser scanning microscopy (CLSM) images of GOPE at a volume fraction (φ) of 0.5 (G).

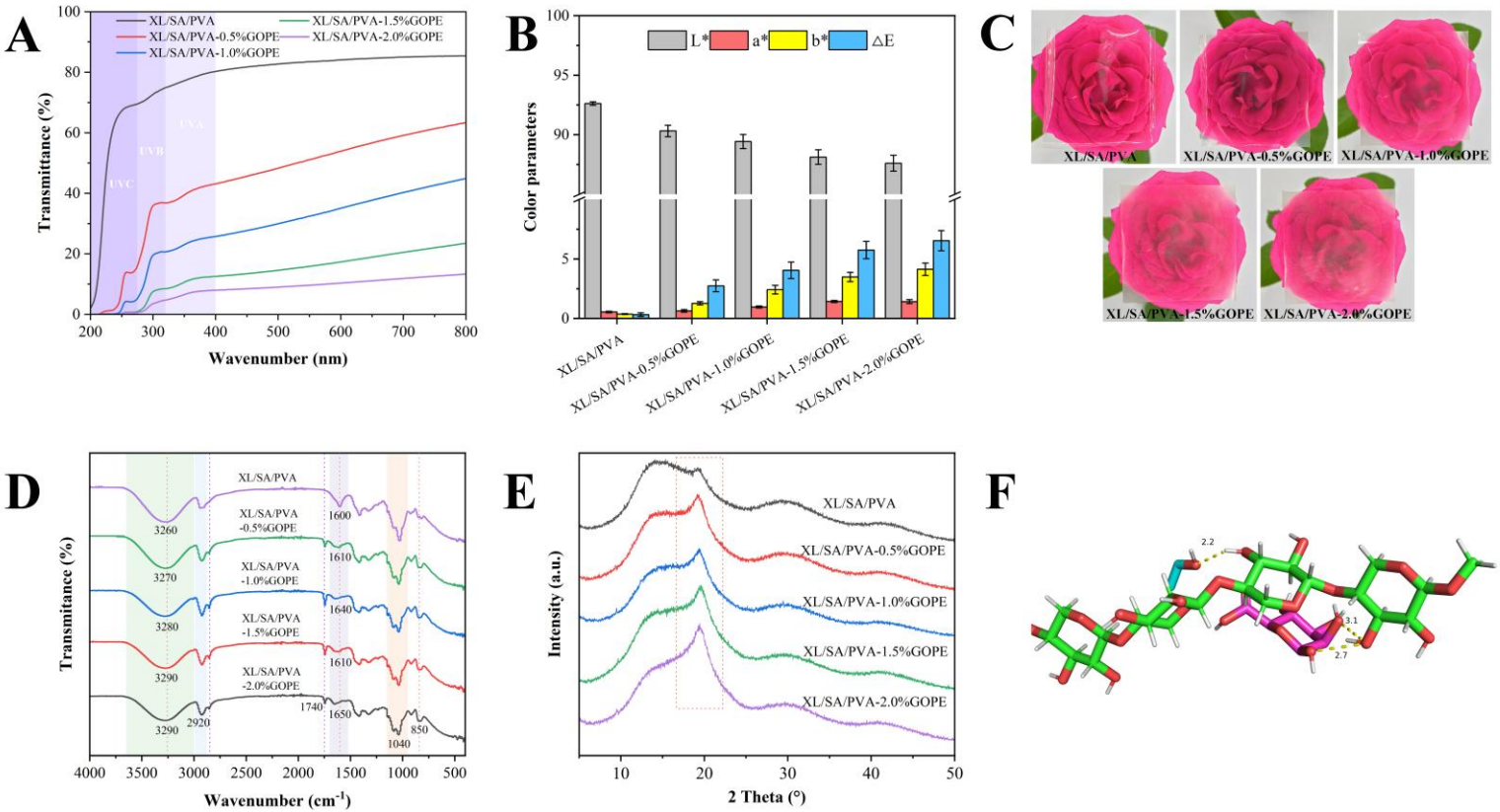

Fig. 3. UV transmittance (A), color parameters (B), digital photographs (C), FT-IR (D), and XRD spectra (E) of XL/SA/PVA films containing different concentrations of GOPE; 3D images of molecular docking simulations of xylan, sodium alginate, and PVA (F). The green molecules, purple molecules and blue molecules represent xylan, sodium alginate, and PVA, respectively, and the yellow dotted lines represent hydrogen bonding interactions.

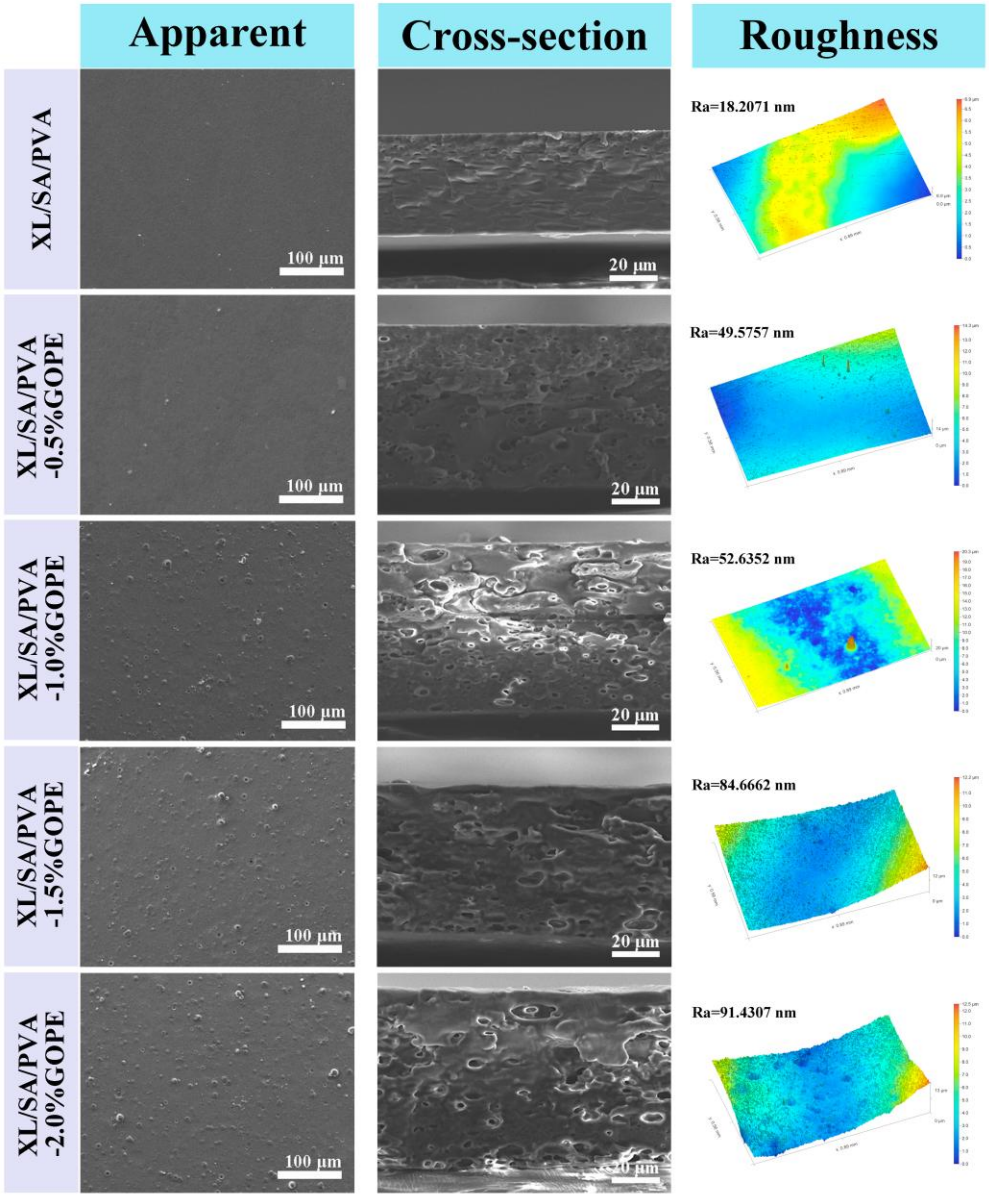

Fig. 4. SEM micrographs (surface and cross-section) and 3D surface profiles of XL/SA/PVA films containing different concentrations of GOPE.

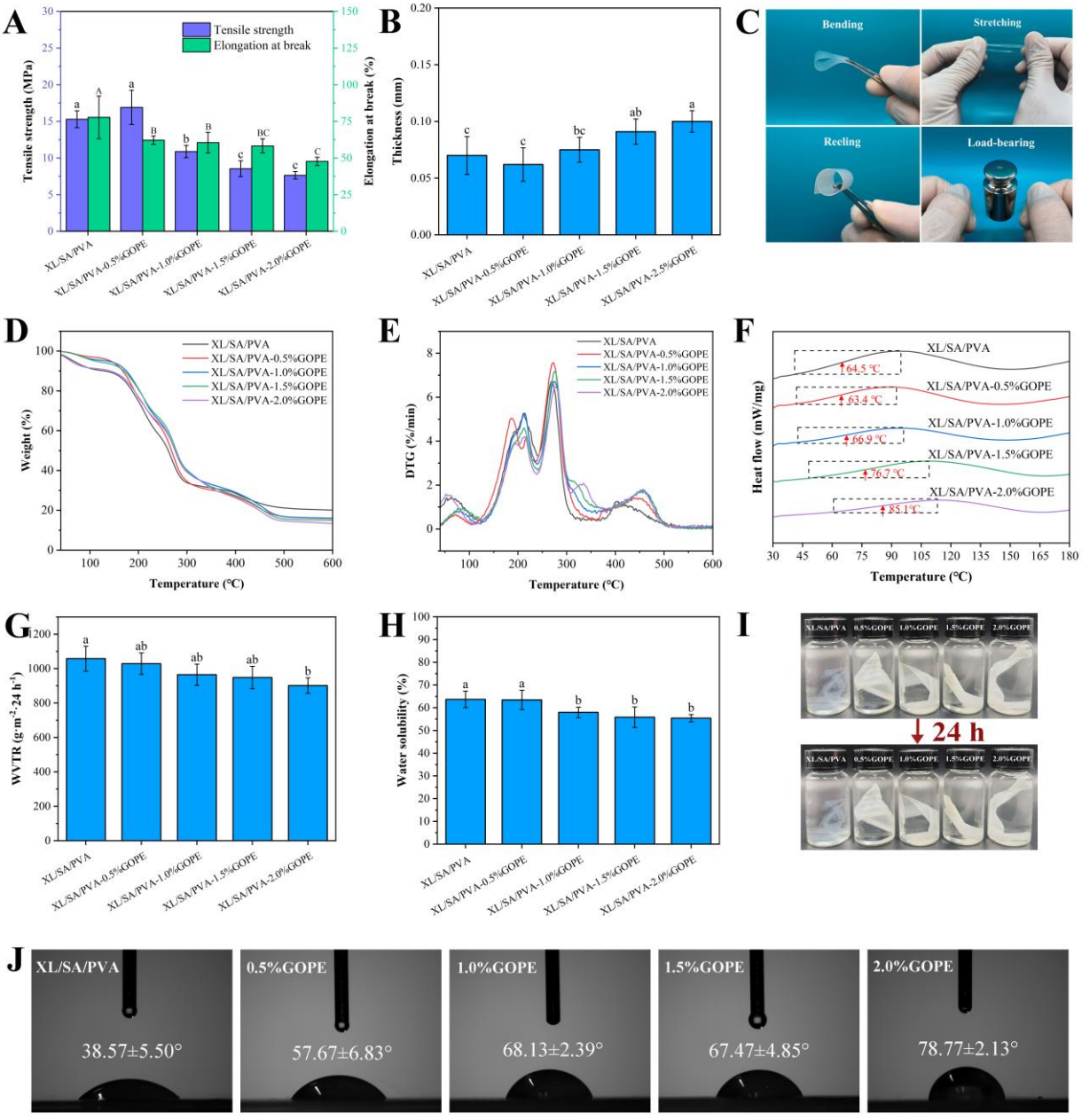

Fig. 5. Tensile strength (TS) and elongation at break (EAB) (A), thickness (B), deformation behavior (C), thermogravimetric (TG) (D) and derivative thermogravimetric (DTG) curves (E), differential scanning calorimetry (DSC) thermograms (F), water vapor transmission rate (WVTR) (G), water solubility (WS) (H), photographs after water immersion (I), and water contact angle (WCA) (J) of XL/SA/PVA films containing different concentrations of GOPE. Different superscripts indicate

significant differences ($P < 0.05$).

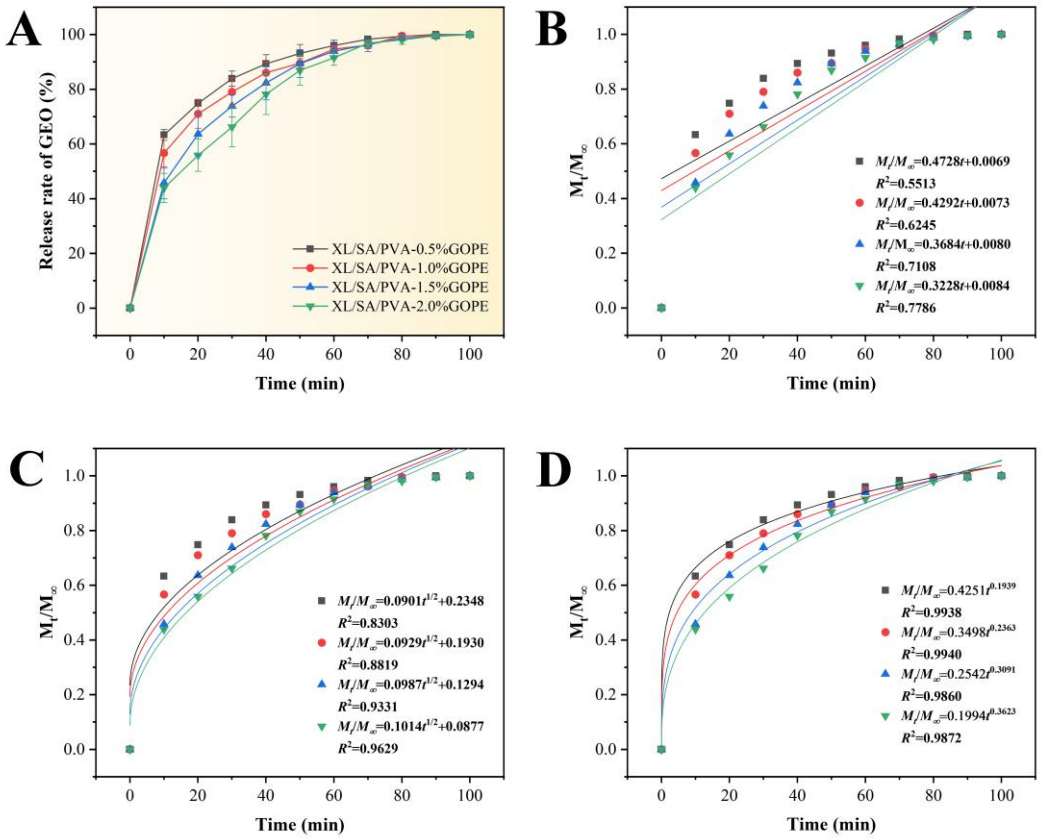

Fig. 6. Release behavior (A) and release kinetics fitting of ginger essential oil (GEO) in different composite films: Zero-order release kinetics model (B), Higuchi release kinetics model (C) and Ritger-Peppas release kinetics model (D).

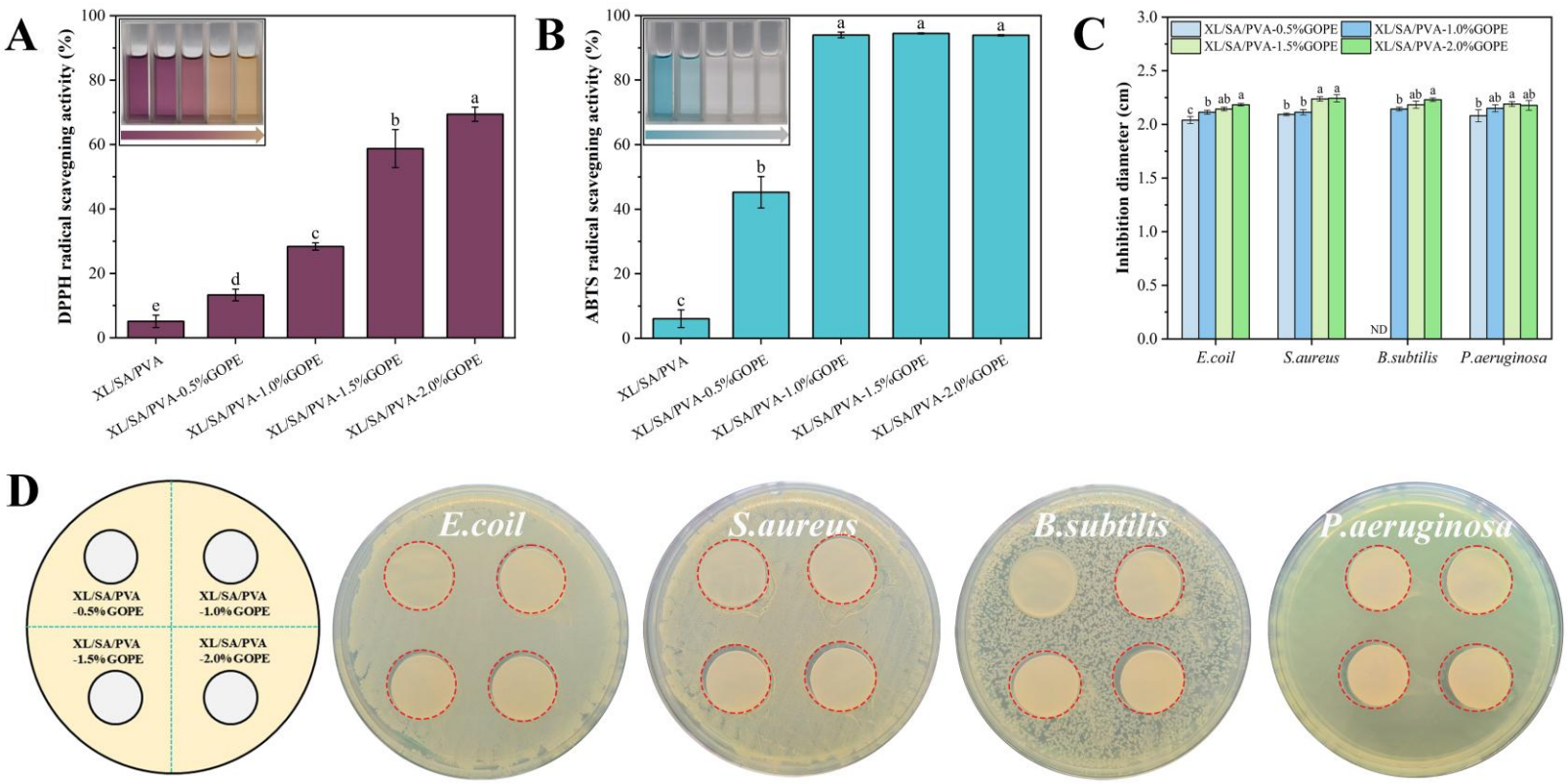

Fig. 7. DPPH (A) and ABTS (B) radical scavenging activity, inhibition diameter against bacteria (C), and antibacterial pictures (D) of XL/SA/PVA films containing different concentrations of GOPE. Different superscripts indicate significant differences ($P < 0.05$).

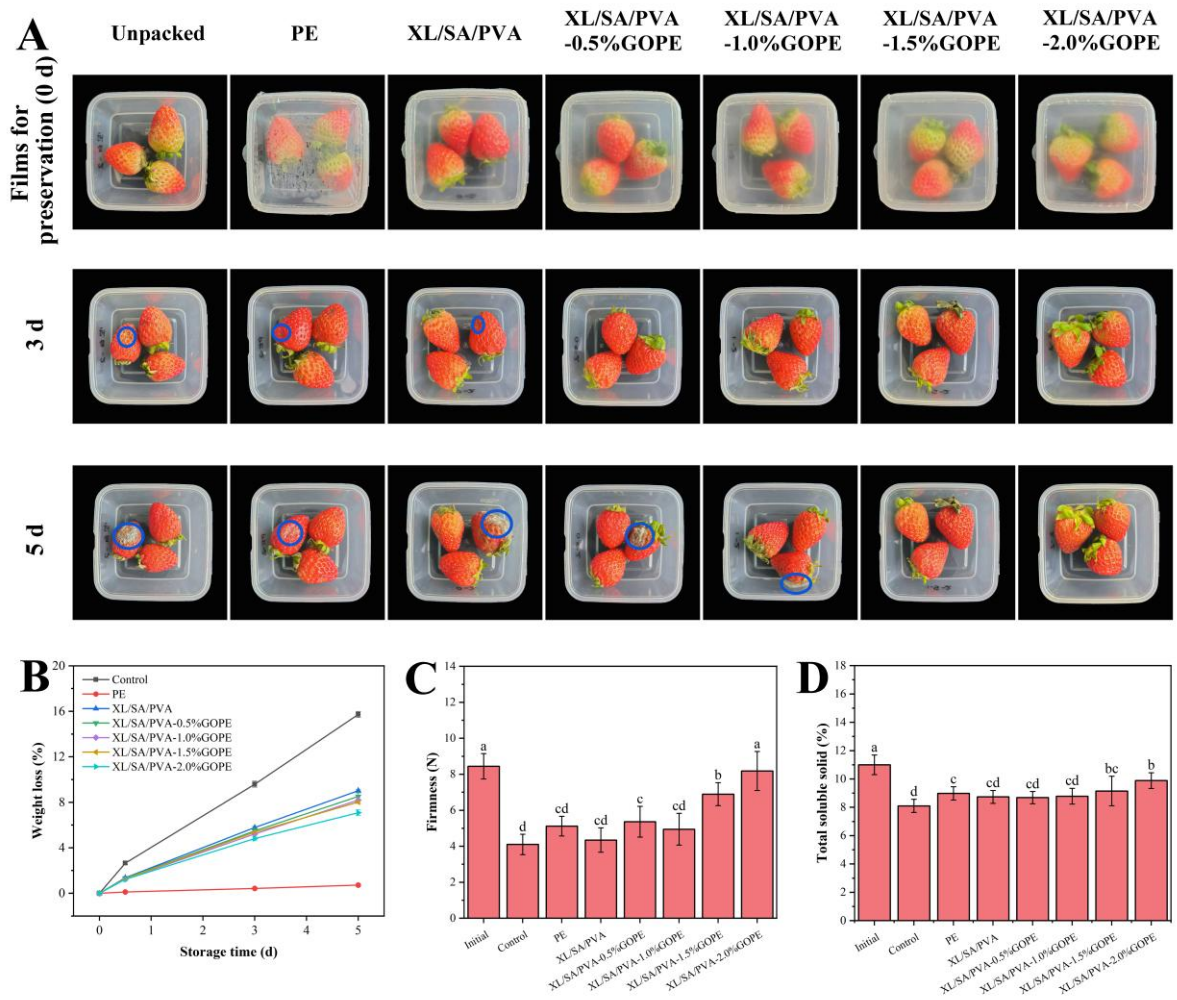

Fig. 8. Changes in visual appearance (A), weight loss (B), firmness (C) and total soluble solids (D) of strawberries during storage in different films. Different superscripts indicate significant differences ($P < 0.05$). Decay regions are highlighted with bold circles for clarity.

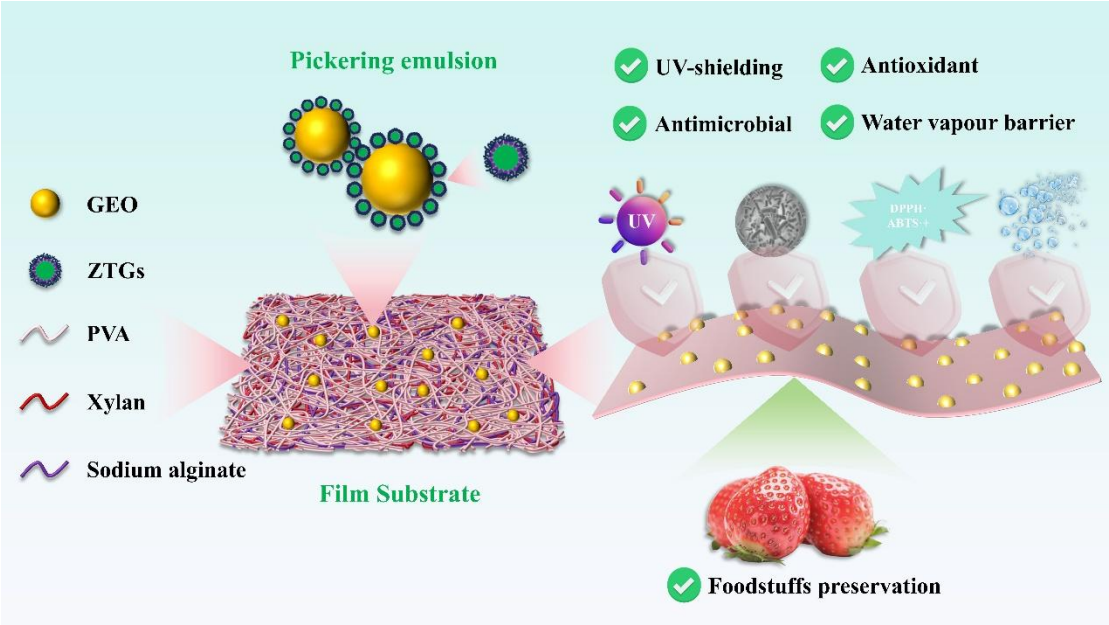

Highlights

• Ternary nanoparticles (ZTGs) were synthesized from zein, tannic acid, and gum Arabic.

• ZTGs effectively stabilized Pickering emulsions of ginger essential oil (GOPE).

• GOPE was blended into xylan/ sodium alginate/PVA matrices to fabricate active films.

• The active films exhibited antioxidant, antibacterial, and preservation effects.

• The application of GOPE in active films demonstrated considerable potential.